J Fluoresc (2017) 27:1277–1284
DOI 10.1007/s10895-017-2059-5

ORIGINAL ARTICLE

Synthesis and Characterization of Surface Modified, Fluorescent and Biocompatible ZnS Nanoparticles with a Hydrophobic Chitosan Derivative

B. Jothimani[1] · **S. Sureshkumar**[1] · **B. Venkatachalapathy**[2]

Received: 22 December 2016 / Accepted: 19 February 2017 / Published online: 23 March 2017

Abstract The introduction of a hydrophobic moiety on chitosan enhances the self-assembling properties, mucoadhesion, the permeability of the macromolecule and aids in target specific delivery. Our group synthesized a hydrophobic *trans* N-(6,6-Dimethyl-2-hepten-4-ynyl)chitosan derivative (CSD) and studied the surface modification of ZnS nanoparticles in a single pot reaction. X-ray diffraction studies and FESEM imaging confirms the nano size and morphology of the surface modified Zinc sulfide nanoparticles (ZnS-CSD NPs). The proposed ZnS-CSD NPs showed excellent emission at 457 nm. Photostability studies indicate that the surface modified ZnS-CSD NPs possess better photostability than Rhodamine B and FITC. Cell viability tests confirmed the biocompatibility of the modified nanoparticles. All these features of ZnS- CSD NPs makes these candidates an excellent choice in a wide range of in vitro or in vivo studies as fluorescent biological labels.

Keywords Biocompatible · Fluorescent · Zinc sulfide · Chitosan · Nanoparticles

Introduction

Human cervical cancer is the fourth most cause of tumor-related deaths [1]. Although imaging techniques such as Positron emission tomography (PET), and Single photon emission computed tomography (SPECT) are available to detect changes at the cellular level, they suffer from spatial resolution. On the other hand, Magnetic resonance imaging (MRI) offers good spatial resolution but lacks imaging at molecular level due to low sensitivity for the detection of contrast agents. To achieve spatial resolution and the sensitivity to detect biochemical events several hybrid systems with morphological and molecular imaging capabilities are exploited [2]. Nanoparticle-based imaging agents known as exogenous optical contrast agents emerged as promising nano-sized fluoroprobes. They possess high surface to volume ratio, excellent photostability, and optical properties to image at cellular levels [3]. Among many nanoparticles in use, ZnS has its unique features such as biocompatibility and wide band gap energy of 3.6–3.9 eV. Moreover, ZnS exhibits luminescence at room temperature [4, 5]. Though ZnS nanoparticles possess some unique properties, the photostability remains a challenge. For fluorescence imaging, the material should exhibit stable and intense luminescence. To improve the photostability, the surface of ZnS modified with suitable capping agents like 3-Mercaptobutyric Acid, Chitosan, and PVA [6–8]. Particularly several works attracted chitosan as capping agent [9, 10].

Chitosan is a linear, semi-crystalline polysaccharide, composed of (1➔ 4) -2-amino-2-deoxy-β-D-glucosamine unit, is the most abundant bio-based polymer next to cellulose. This biopolymer have been extensively studied in several biomedical applications, because of its biocompatible and biodegradable nature [11]. The degradation products of chitosan are non-toxic and non-carcinogenic [12, 13]. In the field of nanotechnology, chitosan and its derivatives have been studied in drug delivery, tissue engineering, mucoadhesion and many other applications [14]. Biocompatibility and biodegradability are one of the key parameters decide the utility of the

✉ B. Venkatachalapathy
bv1461967@gmail.com

[1] Department of Chemistry, Rajalakshmi Engineering College, Thandalam, Chennai 602105, India

[2] SRM Easwari Engineering College, Ramapuram, Chennai 600089, India

nanoparticles systems in biological applications. These properties of chitosan are well studied and documented by both in vitro and in vivo studies [15–18].

Chitosan has attracted several works in nanoparticle synthesis for surface modifications of an inorganic core. In further improvement, chitosan is modified structurally to target specific applications. Self-assembly over a core is the main objective of structural modifications because, in this spontaneous process organized structures are formed with specific functions and properties without further processing. In the multi-component self-assembling process, the molecular structure plays an important role driven by electrostatic interactions or hydrogen bonds between chitosan and the other molecule [19]. One of the main advantages of the self-assembly is its cost-effectiveness to prepare hybrid nanoparticles with an inorganic core and organic surface modifications. The Self -assembly process is a bottom-up approach in which parameters such as temperature, reaction time, stoichiometric mole ratios can be controlled to define the size and morphology. Also, the self-assembly process of chitosan and its derivatives resembles many biological molecules (DNAs, RNAs).

The introduction of moieties such as alkyl [20], phthaloyl [21], polyester [22], fatty acid [23], cholesterol [24] functionality on chitosan enhances the hydrophobic nature to achieve the intended purpose. Based on our current research work, we communicate a surface modifying agent based on chitosan with structurally significant hydrophobic side chain which is new and not reported elsewhere. In the current research work, we modified chitosan using *trans* N-(6,6-Dimethyl-2-hepten-4-ynyl) side chain (Fig. 1). The chemical modification attempted on chitosan provides a hydrophobic moiety to the structure of native chitosan which enhances the self-assembling capabilities by increasing intermolecular hydrophobic interaction between the segments.

In the present work, the side chain formed by direct N-alkylation eliminates toxic by-products observed in the Schiff base route to synthesize similar products [25]. In the Schiff base route, Chitosan reacted with aldehydes or ketones to yield corresponding aldimine or ketimine. Sodium borohydride($NaBH_4$), Sodium cyanoborohydride($NaBH_3CN$) are used to reduce the imine to get the N-alkyl derivative. $NaBH_3CN$ is widely used in reductive alkylation because of selectivity it offers in reactions. However, it generates toxic by-products such as HCN or NaCN [26]. In the direct N-alkylation of Chitosan, no such toxic by-products are envisaged. In addition to the synthetic advantage, the presence of trans-hydrogen, alkene and alkyne functionalities in the structure of the ZnS –CSD NPs will aid in adapting to the complex, undefined biological domains.

The N-alkylation attempted would enable the derivative soluble in water even at higher degree of substitution (DS) due to amphiphilic nature of the molecule and possible protonation of the resultant secondary amine group, though the side chain is hydrophobic [27].Whereas in hydrophobic modifications through N-acylations of chitosan solubility in aqueous conditions is limited beyond certain DS [28]. With this background and objective of modifying the surface of ZnS nanoparticles based on enhanced self-assembly, *trans* N-(6,6-Dimethyl-2-hepten-4-ynyl) chitosan used in the current work would provide nanostructures in which the hydrophobic entities can assemble away from the core ZnS. Further conjugation of ZnS- CSD NPs with suitable cancer targeting ligand like folic acid through EDC coupling chemistry is possible. This modification would make these nanoparticles utilisable in detecting other forms of cancer [29, 30]. Application of proposed ZnS –CSD NPs in drug delivery needs to be explored. Because of its fluorescence properties the synthesized nanoparticle may function as theranostic agent [31].

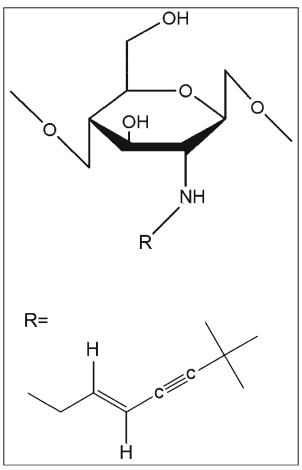

Fig. 1 Structure of trans N-(6,6-Dimethyl-2-hepten-4-ynyl)chitosan

Materials and Methods

Materials

Chitosan powder (MW 50 kDa, 100% deacetylation) of crab shell origin was supplied by Panvo Organics Pvt. Ltd., (Chennai, India). 1-chloro–6, 6–dimethyl–2–hepten–4-yne was purchased from Hangzhou Volant Technology Co Ltd. (Hangzhou, China). Zinc acetate, Sodium sulfide, Sodium Carbonate, Sodium hydroxide, Glacial Acetic acid, Acetone, Methanol and other reagents were purchased from Avantor Performance Materials India Ltd. (Thane, India).

Synthesis of *trans* N-(6,6-Dimethyl-2-Hepten-4ynyl) chitosan (CSD)

Chitosan (3.0 g, 0.0186 mol) was dissolved in 3% *w/v* aqueous acetic acid (300 ml) under mechanical stirring for two hours at room temperature. pH of the mass was adjusted to 6.0 using 5%*w/v* sodium hydroxide solution. Sodium

carbonate (3.0 g, 0.026 mol) was added and under vigorous stirring 1-chloro–6,6–dimethyl–2–hepten–4yne (3.0 g 0.019 mol) was introduced over 10 min. The heterogeneous reaction mixture temperature was raised to 90 °C and stirred for 4 h. The product was precipitated by adding to acetone (1.5 l) under good mixing, filtered and washed thoroughly with methanol. The collected precipitate dried under vacuum at 50 °C. The yield was 3.35 g (64.42%). Figure 2a provides reaction methodology.

Synthesis ZnS, ZnS-CSD and ZnS-CS Nanoparticles

0.1 M of $Zn(OAc)_2$, 0.01% *w*/*v* CSD in aqueous acetic acid were taken in a beaker. With constant stirring (1000 rpm), 0.1 M Na_2S aqueous solution (2.5 ml) was added, and the pH of the solution was raised to 10 by adding 1 M NaOH. This mixture was stirred at 60 °C for 3 h and cooled to room temperature. The precipitate was collected by centrifugation (2500 rpm) and washed thoroughly with milliQ water and dried under vacuum to get ZnS-CSD nanoparticles. The same procedure was followed using various concentrations of CSD (0.02, 0.03, 0.04 and 0.05% *w*/*v*) to modify ZnS NPs. In another experiment, surface modification of ZnS using 0.01% aqueous solution of native chitosan was carried to get ZnS-CS nanoparticles. The unmodified ZnS was prepared by following the same procedure without the addition of surface modifiers [32].

Characterization

X-ray diffraction (XRD) of the prepared samples were done using Bruker D8 diffractometer with Cu Kα radiation (λ = 1.5418 Å) within the the2θ range of 10–80°. FTNMR studies were carried out using (BruckerAvance, 500 MHz).FTIR of the samples recorded with Perkin-ElmerSpectrum II. Elemental analysis was performed using a Perkin Elmer elemental analyzer, (Model 2400), Field Emission Scanning Electron Microscopy (FESEM)

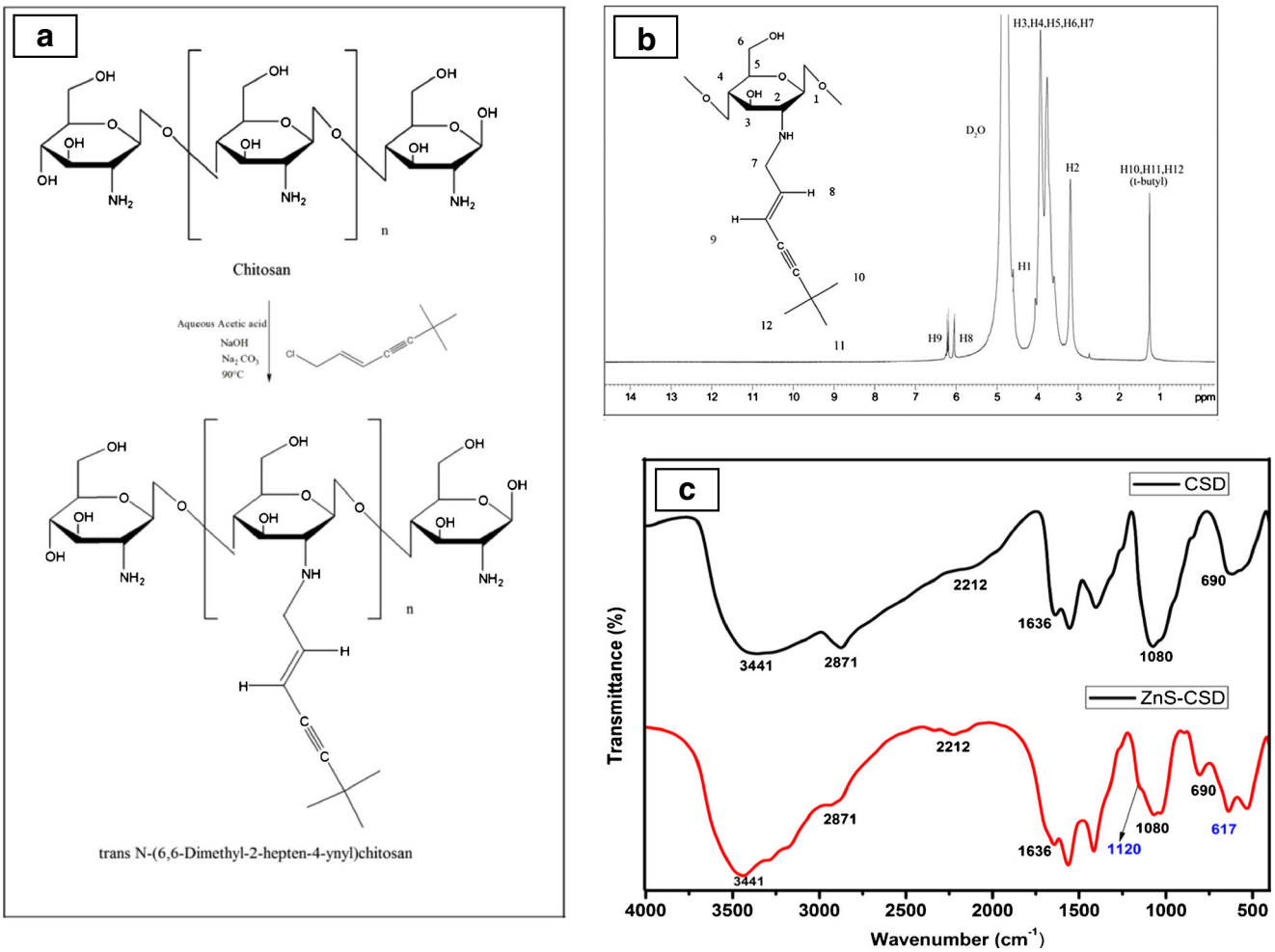

Fig. 2 (**a**), (**b**) shows the scheme of synthesis and ^{1}HNMR spectra of *trans* N-(6, 6-Dimethyl-2-hepten-4ynyl) chitosan respectively. (**c**) FTIR spectrum of CSD and ZnS-CSD nanoparticles

and Energy Dispersive Analysis X-Ray (EDAX) of ZnS-CSD NPs were investigated using CARLZEISS (FESEM-SUPRA 55). Fluorescence spectra were recorded on Varian Cary-Eclipse fluorescence spectrophotometer.

Cell Culture and in Vitro Cytotoxicity Studies

HeLa cells were procured from National Centre for Cell Sciences (NCCS, Pune, India) and cultured in DMEM supplemented with 10% fetal bovine serum (FBS) in the presence of penicillin and streptomycin in a humidified incubator with 5% CO_2 at 37 °C. Cell viability was assessed using MTT assay as reported earlier with slight modifications [33, 34].

Results and Discussions

The degree of substitution (DS) of a chitosan derivative is calculated by comparing C and N molar ratio obtained from the elemental analysis data. Elemental analysis of CSD was calculated for $(C_6H_{11}NO_4)_{0.78}(C_{15}H_{23}NO_4)_{0.22}$ 0.47 H_2O. Calculated: C,48.89: H,7.51:N,7.15. Obtained results: C,48.79: H,7.87:N,6.87. Based on the elemental analysis, DS was calculated and provided in Table 1. From the data, it can be found that there is an increase in carbon percentage on CSD which confirmed the substitution. From the C/N molar ratios, the increase in mass was obtained as 2.285 g/mol and DS was found to be 0.25. The heterogeneous nature of the synthesis step followed could have limited the substitution.

The proton NMR spectra were recorded to confirm the structure of CSD in D_2O/DCl. Figure 2b shows the proton NMR spectra of CSD. The chemical shifts assigned for the respective protons are summarized in Table 2.

No proton peak of the CH_2 group (H7) attached to the Nitrogen observed. This observation could be because of the merger of the peak in the region 3.0–4.0 where the pyranose protons (H3toH6) of chitosan appear. FTNMR studies confirmed the structure of CSD.

Figure 2c shows the FT-IR spectra of CSD and ZnS-CSD NPs. The characteristic IR frequencies of CSD were assigned as follows: 3441 cm^{-1} was attributed to the stretching vibrations of –OH group. The peak at 2871 cm^{-1} was assigned to – CH stretching of pyranose moiety. The –NH deformation peak appeared at 1636 cm^{-1}. The band at 1094 cm^{-1} was due to the –CO stretching. The C ≡ C (alkyn) vibrational band was observed at 2212 cm^{-1}. All the observed IR bands confirmed the N-alkylation on Chitosan. For ZnS-CSD NPs, the stretching

Table 1 Degree of substitution of CSD

	C(%)	N(%)	m(C)/m(N)#	DS
Chitosan	44.71	8.69	6.0	---
CSD	48.79	6.87	8.285	0.25*

m represents number of moles

*refers to 25% substitution with respect to free amine group of CSD

Table 2 ^{1}HNMR chemical shifts of CSD

Chemical shift δ (ppm)	Mutiplicity	Assignment
1.25	singlet	H10, H11, H12 (t-butyl)
3.2	singlet	H2
3.5–4.1	multiplet	H3, H4, H5, H6, H7
4.6	singlet	H1
4.8	—	D_2O
6.1	multiplet	H8 (trans proton)
6.2	multiplet	H9 (trans proton)

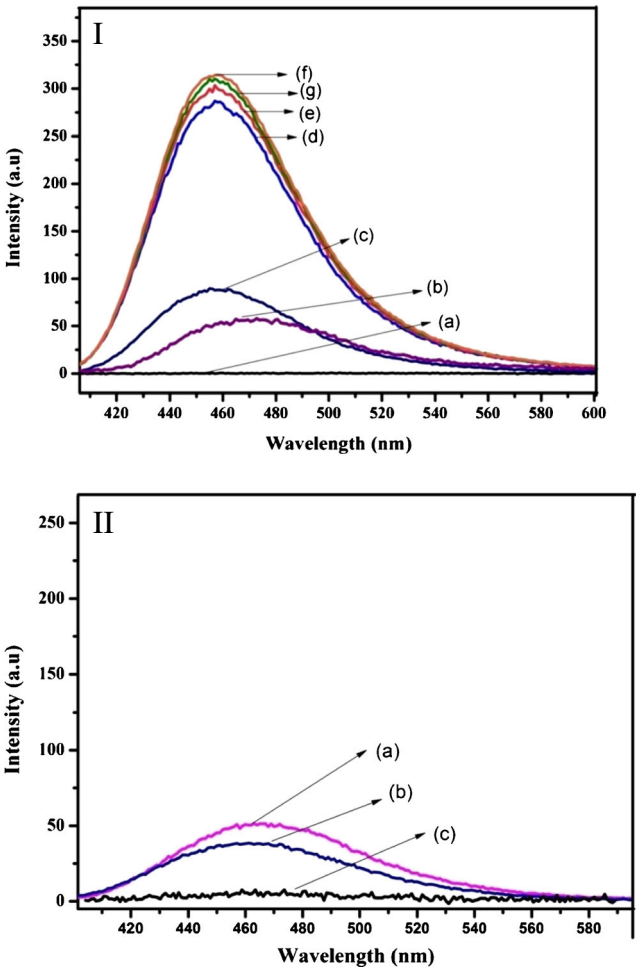

Fig. 3 **(I)** Fluorescence emission spectra of CSD modified ZnS NPs (*a*) CSD, (*b*) ZnS, (*c*) 0.01% (*w/v*) CSD modified ZnS, (*d*) 0.02% (*w/v*) CSD modified ZnS, (*e*) 0.03% (*w/v*) CSD modified ZnS, (*f*) 0.04% (*w/v*) CSD modified ZnS and (*g*) 0.05% (*w/v*) CSD modified ZnS. (**II**). Fluorescence emission spectra of native chitosan modified ZnS nanoparticles, (*a*) Pure ZnS, (*b*) Native Chitosan (0.01%) modified ZnS nanoparticles, (*c*) Native chitosan

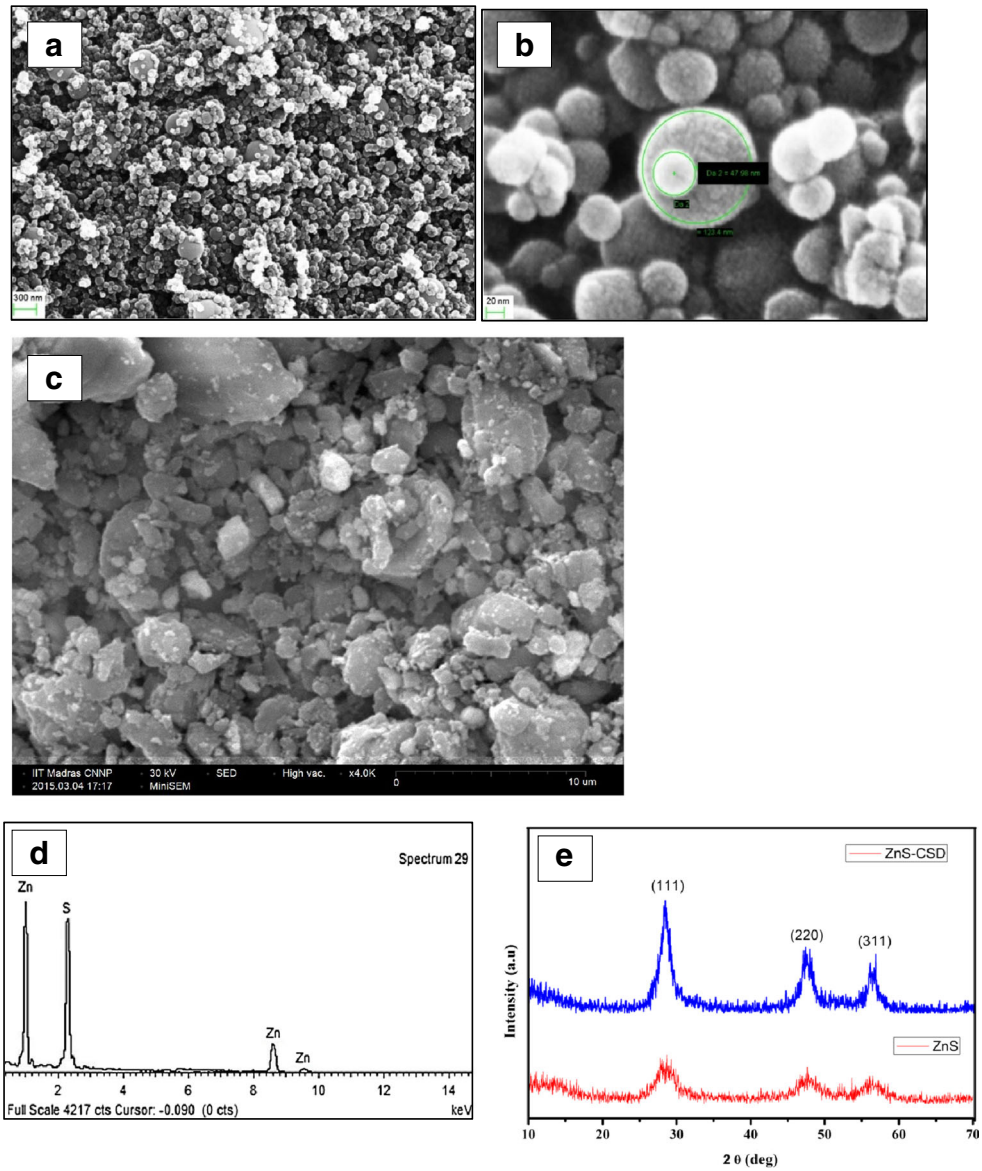

Fig. 4 (**a**) FESEM image of ZnS-CSD NPs (**b**) Magnified image of ZnS-CSD NPs, (**c**) FESEM images of native Chitosan (0.01%) modified ZnS nanoparticles, (**d**) EDAX of ZnS-CSD nanoparticles (**e**) XRD pattern of unmodified ZnS and ZnS-CSD nanoparticles

vibrations of ZnS appeared at 1120 cm^{-1} along with all the characteristic peaks of CSD which confirmed the nanoparticles formation [35].

Figure 3 shows the fluorescence spectra of ZnS, ZnS-CSD and ZnS-CS nanoparticles. The fluorescence spectra in Fig. 3I (a) shows fluorescence of CSD. Figure 3I (b) shows fluorescence spectrum of unmodified ZnS nanoparticle. Figure 3I (c-g) shows the impact on the fluorescence intensity of ZnS-CSD NPs with the increase in CSD concentration used to modify ZnS NPs surface. When CSD concentration increased up to 0.04%*w/v*, fluorescence intensity increased. Further, with an increase in the CSD concentration to 0.05% *w/v*, the fluorescence intensity decreased. From the fluorescence studies, the optimized concentration of CSD to prepare ZnS-CSD NPs was identified as 0.04% *w/v*. It was also observed that CSD played an important role in controlling the size of the ZnS-CSD NPs and this could be possible because of combined effect of intramolecular hydrogen bonding, electrostatic interactions and Van der waals forces exerted by the polymer on ZnS NPs [19]. Later, the optimized concentration (0.04%*w/v*) which showed maximum intensity in fluorescence studies was used in cell imaging. In Fig. 3I (a) blue shift can be observed at 457 nm. Normally, ZnS nanoparticles exhibit enhanced intensity as well as blue shift in the 400-550 nm region which are associated with the surface defects arisen due to the presence of increased vacant surface oxygen sites over the nanomaterial [36, 37]. In the fluorescence studies, the intensity of ZnS-CSD NPs got quenched when CSD concentration increased beyond 0.05% during synthesis. The reason for the decreased fluorescence response with the increase in the concentration of CSD NPs might be due to the self-

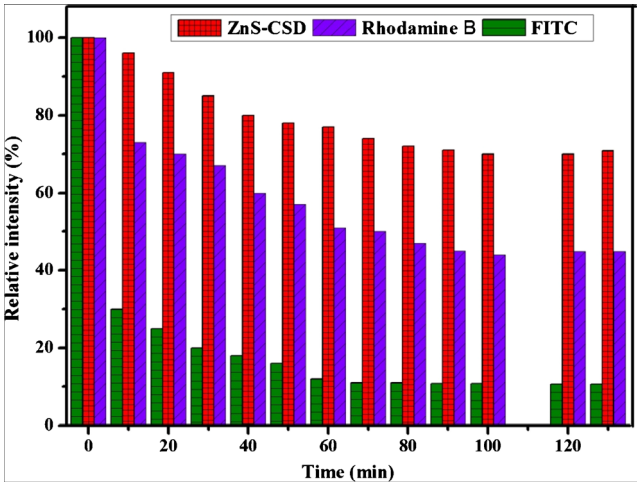

Fig. 5 Photostability comparison of Rhodamine B,FITC and ZnS-CSD NPs under excitation wavelength with 365 nm at different time points (0 to 130 min). Concentration of fluorophore: 20 mg dissolved in 100 ml of milliQ water

quenching effect, which is the result of a collision between the molecules of the fluorophore.

To understand and evaluate the impact of the N-substitution of chitosan on surface modification of ZnS, fluorescence and morphology studies were carried out for the native chitosan modified ZnS nanoparticles(CS-ZnS NPs). Figure 3 (II) presents the emission spectrum of ZnS-CS NPs which indicated that even at the lowest concentration of 0.01% chitosan the intensity of fluorescence is not significant. Quenching even at this lowest concentration could be due to polycationic nature of the polymer. Presence of hydroxyl and amine groups in chitosan would exert strong the inter and intramolecular hydrogen bonding and other non covalent interactions. In a net effect, a non uniform self assembly of chitosan over ZnS NPs might happen which could have impacted the fluorescence [19].

Figure 4 exhibits FESEM image, energy dispersive X-Ray analysis (EDAX), and XRD of ZnS-CSD nanoparticles. The morphology of ZnS-CSD NPs was spherical as observed from Fig. 4a and the particle sizes ranged from 40 to 130 nm as shown in Fig. 4b. FESEM studies confirmed that CSD played an important role in controlling the shape and size of ZnS-CSD NPs. Figure 4c shows the morphology of CS-ZnS NPs. From the FESEM images of CS-ZnS NPs, we can observe the undefined particle shape and uncontrolled non-uniform particle size. This indicate that the surface modification of ZnS NPs with modified chitosan lead to NPs with uniform morphology. Figure 4d shows EDAX spectrum of ZnS-CSD which confirmed the stoichiometric purity of nanoparticles.

Figure 4e shows XRD pattern of ZnS and ZnS-CSD. The diffraction peaks at 28.5, 47.5 and 56.1 correspond to the lattice planes of (111), (220) and (311) which can be observed in both ZnS and ZnS-CSD.The crystalline XRD pattern matches very well with published literature of ZnS nanoparticles [38–40]. All the corresponding diffraction peaks matched very well with the cubic zinc blende structure (JCPDS No. 05–0566). The absence of any other peaks indicated that the prepared materials were free from impurities. ZnS –CSD peak intensities increased when compared to unmodified ZnS, suggesting that the crystallite size of ZnS decreased as a result of the modification with CSD. Peak broadening of ZnS and ZnS-CSD indicated the nanocrystalline nature of the synthesized materials. Using Debye-Scherrer formula (Eq. 1), crystallite size was calculated.

$$D = k\gamma/\beta\cos\theta \quad (1)$$

Where D is the mean grain size, k is constant, λ is the X-ray wavelength (1.54 A° for Cu-Kα), β is the full width at half maximum of the diffraction peak, and θ is the Bragg angle. The average crystallite sizes of ZnS and ZnS-CSD were found as 80 nm and 40 nm respectively which was due to passivation of CSD over ZnS surface.

Photostability of a fluorescence probe is one of the essential parameters decides the effective usage of the probe in imaging applications [41]. In particular, extended time imaging of cancer cells or tissues is a key parameter significant in biological studies for a proper understanding of the malignancy Fig. 5 shows the photostability of ZnS-CSD NPs along with fluorescein isothiocyanate (FITC), and Rhodamine B. To evaluate the photostability of the ZnS-CSD NPs, 0.02% *w/v* ZnS-CSD solution was irradiated constantly using UVlamp. The emission spectra of tested samples were measured from 0 to 130 min at every 10 min time interval. As shown in Fig. 5, ZnS- CSD NPs exhibits significant photostability when compared with the other two dyes studied even after 130 min of UV exposure. Hence, it was concluded that ZnS-CSD NPs has significant photostability in comparison with Rhodamine B and FITC.

Figure 6 shows the cell viability study results using Methyl thiazolyl tetrazolium (MTT) assay, and Fig. 7 shows the

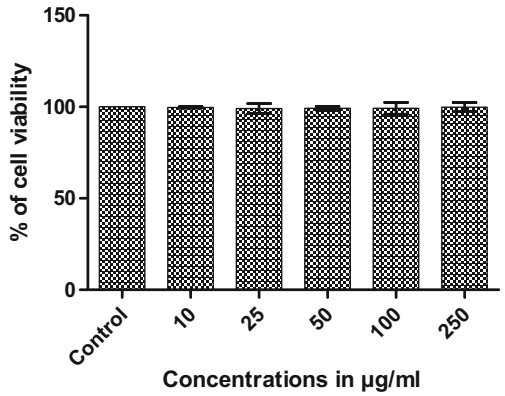

Fig. 6 Cell viability of ZnS-CSD nanoparticles on HeLa cells

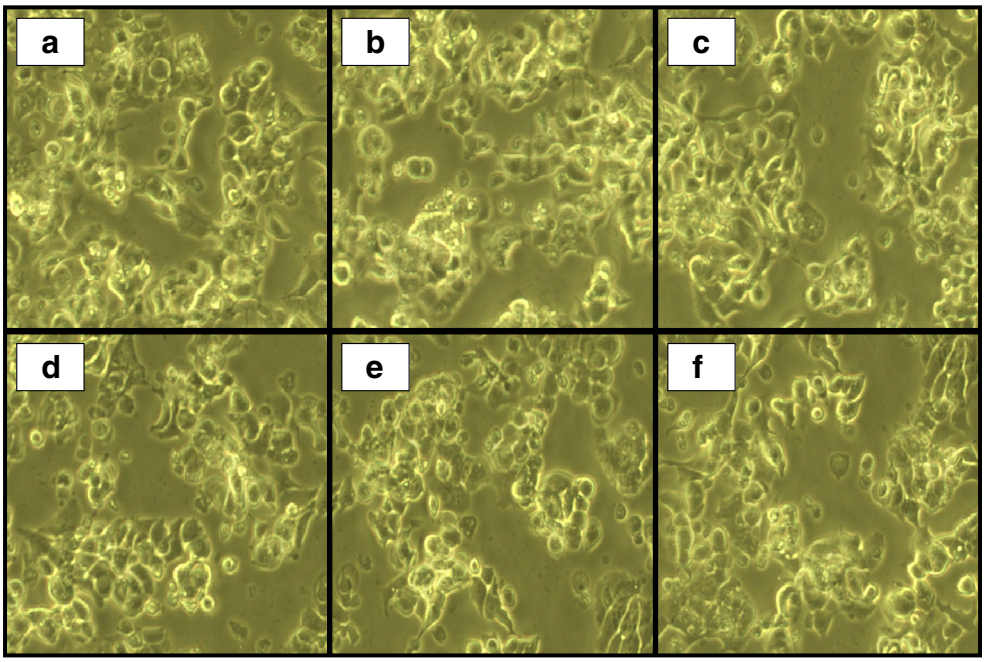

Fig. 7 Photographs of HeLa Cell viability Co-Cultured with ZnS-CSD NPs (**a**) Control HeLa, (**b**) ZnS-CSD NPs 10 μg/ml, (**c**) ZnS-CSD NPs 25 μg/ml, (**d**) ZnS-CSD NPs 50 μg/ml, (**e**) ZnS-CSD NPs 100 μg/ml and (**f**) ZnS-CSD NPs 250 μg/ml

photographs of ZnS-CSD co-cultured with HeLa cells at different concentrations. Cell toxicity assay exhibited that even at a concentration of 250 μg/ml, more than 90% of cells were viable. Hence ZnS-CSD NPs can be used as a fluoroprobe in cancer cell imaging and as a carrier molecule in drug delivery in the future.

Investigations of ZnS-CSD NPs reported in the current work support the fact that surface modification of ZnS NPs using the chitosan derivative (CSD) lead to better self-assembly which yielded the nanoparticles with uniform size and morphology. The findings correlate very well with the polymer assisted surface modification results published in the literature [42].

Conclusions

In summary, the surface of the ZnS nanoparticle was successfully modified using *trans*N-[6,6,-Dimethyl-2-hepten-4-ynyl]chitosan. Fluorescence properties of the surface modified nanoparticles was studied at room temperature. ZnS-CSD NPs exhibited emission at 457 nm and the photostability of ZnS-CSD was found better when compared with Rhodamine B and FITC. The optimized concentration to modify ZnS surface was identified as 0.04% to achieve significant fluorescence. The sizes of ZnS-CSD nanoparticles were in the range of 40-130 nm as observed from FESEM and showed spherical morphology. XRD studies confirmed the cubic zinc blende structure of ZnS-CSD and size of nanoparticles. MTT assay studies confirmed the biocompatibility of ZnS-CSD NPs. Easy of synthesis and better photostability of ZnS-CSD NPs could make these candidates a promising fluorescence probe to image cancer cells both in Vitro and in Vivo.

References

1. Stewart BW, Wild CP (Eds.): World Cancer Report (2014) International Agency for Research on Cancer (IARC), 2014. 630pp
2. Prashant A, Gustav JS, Klaas N (2010) Chitosan-based systems for molecular imaging. Adv Drug Deliv Rev 62:42–58
3. Chan WC, Maxwell DJ, Gao X, Bailey RE, Han M, Nie S (2002) Luminescent quantum dots for multiplexed biological detection and imaging. Curr Opin Biotechnol 13(1):40–46
4. Hwang JM et al (2005) Preparation and characterization of ZnS-based monocrystalline particles for polymer light-emitting diodes. Curr Appl Phys 5(1):31–34
5. Cho H et al (2009) Highly flexible organic light-emitting diodes based on ZnS/Ag/WO_3 multilayers transparent electrodes. Org Electron 10(6):1163–1169
6. Ji Z, Xiao-X F, Jin Q, Zhi-F Z, Yan-M M, Gui-Q Y (2016) A sensitive phosphorescence method based on MPA-capped Mn-doped ZnS quantum dots for the detection of diprophylline. New J Chem 40:3857–3862
7. Haiying W, Xiaofeng L, Yiyang Z, Ce W (2006) Preparation and characterization of ZnS: Cu/PVA composite nanofibers via electrospinning. Mater Lett 60:2480–2484
8. Pallab S, Shivendra BP, Arun C, Siddhartha SG (2010) Incorporation of gene therapy vector in chitosan stabilized Mn^{2+}-doped ZnS quantum dot. Mater Lett 64:2534–2537
9. Haizhen H, Xiurong Y (2004) Synthesis of polysaccharide-stabilized gold and silver nanoparticles: a green method. Carbohydr Res 339:2627–2631

10. Sugunan A, Thanachayanont C, Dutta JG (2005) Heavy metal ion sensors using chitosan-capped gold nanoparticles. Sci Technol Adv Mater. doi:10.1016/j.stam.2005.03.007
11. Alves NM, Mano JF (2008) Chitosan derivatives obtained by chemical modifications for biomedical and environmental applications. Int J Biol Macromol 43:401–414
12. Muzzarelli RAA (1997) Human enzymatic activities related to the therapeutic administration of chitin derivatives. Cell Mol Life Sci 53:131–140
13. Bersch PC, Nies B, Liebendorfer A (1995) Evaluation of the biological properties of different wound dressing materials. J Mater Sci Mater Med 6:231–240
14. Sudheesh KS, Mishra AK, Omotayo AA, Bhekie BM (2013) Chitosan-based nanomaterials: a state-of-the-art review. Int J Biol Macromol 59:46–58
15. Bhattarai N, Gunn J, Zhang M (2010) Chitosan-based hydrogels for controlled, localized drug delivery. Adv Drug Deliv Rev 62:83–99
16. Gupta K, Ravi Kumar M (2000) Drug release behavior of beads and micro granules of chitosan. Biomaterials 21:1115–1119
17. Hari P, Chandy T, Sharma CP (1996) Chitosan/calcium–alginate beads for oral delivery of insulin. J Appl Polym Sci 59:1795–1801
18. Hirano S (1999) Chitin and chitosan as novel biotechnological materials. Polym Int 48:732–734
19. Yu Y, Shengpeng W, Yitao W, Xiaohui W, Qun W, Meiwan C (2014) Advances in self-assembled chitosan nanomaterials for drug delivery. Biotechnol Adv 32:1301–1316
20. Huo M, Zhang Y, Zhou J, Zou A, Yu D, Wu Y et al (2010) Synthesis and characterization of low toxic amphiphilic chitosan derivatives and their application as micelle carrier for the antitumor drug. Int J Pharm 394:162–173
21. Opanasopit P, Ngawhirunpat T, Chaidedgumjorn A, Rojanarata T, Apirakaramwong A, Phongying S et al (2006) Incorporation of camptothecin into N-phthaloyl chitosan-gmPEGself-assembly micellar system. Eur J Pharm Biopharm 64:269–276
22. Liu K-H, Chen B-R, Chen S-Y, Liu D-M (2009) Self-assembly behavior and doxorubicin-loading capacity of acylated carboxymethyl chitosans. J Phys Chem B 113:11800–11807
23. Lee C, Choi JS, Kim I, Byeon HJ, Kim TH, Oh KT et al (2014) Decanoic acid-modified glycol chitosan hydrogels containing tightly adsorbed palmityl-acylated exendin-4 as a long-acting sustained-release anti-diabetic system. Acta Biomater 10:812–820
24. Wang Y-S, Jiang Q, Li R-S, Liu L-L, Zhang Q-Q, Wang Y-M, Zhao J(2008) Self-assembled nanoparticles of cholesterol-modified O-carboxymethyl chitosan as a novel carrier for paclitaxel. Nanotechnology 19:145101
25. Desbrieres J, Martinez C, Rinaudo M (1996) Hydrophobic derivatives of chitosan: characterization and rheological behavior. Int J Biol Macromol 19:21–28
26. Jayakumar R, Prabakaran M, Muzzarelli RAA (2011) Chitosan for biomaterials II. Springer Verlag, Berlin Heidelberg, pp 24–32
27. Hitoshi S, Yoshihiro S (1999) Chemical modification of chitin and chitosan 2: preparation and water soluble property of *N*-acylated or *N*-alkylated partially deacetylated chitins. Carbohydr Polym 39: 127–138
28. Chan Le T, Monique L,Pompilia I-S, Mircea AM (2003) N-acylated chitosan:hydrophobic matrices for controlled drug release. J.Control.Release 93:1–13
29. Hermanson GT (2013) Bioconjugate Techniques, 3rd Edition, Academic Press, Elsevier.
30. Manjusha EM, Jithin CM, Manzoor K, Nair SV, Tamura H, Jayakumar R (2010) Folate conjugated carboxymethyl chitosan–manganese doped zinc sulfide nanoparticles for targeted drug delivery and imaging of cancer cells. Carbohydr Polym 80:443–449
31. Siti M, Ara SM, Andrew MacKay J (2010) Imaging and drug delivery using theranostic nanoparticles. Adv Drug Deliv Rev 62: 1052–1063
32. Ramanery FP, Mansur AAP, Mansur HS (2013) One-step colloidal synthesis of biocompatible water-soluble ZnS quantum dot/chitosan nanoconjugates. Nanoscale Res Lett 8:512
33. Sureshkumar S, Jothimani B, Sridhar TM, Venkatachalapathy B (2016a) Synthesis and characterization of gadolinium-doped ZnSe quantum dots for fluorescence imaging of cancer cells. RSC Adv 6: 16081–16086
34. Sureshkumar S, Jothimani B, Sridhar TM, Venkatachalapathy B (2016b) Synthesis of hexagonal ZnO-PQ7 nanodisks conjugated with folic acid to image MCF −7 cancer cells. J Fluoresc. doi:10.1007/s10895-016-1932-y
35. Ummartyotin S, Bunnak N, Juntaro J, Sain M, Manuspiya H (2012) Synthesis and luminescence properties of ZnS and metal (Mn, Cu)-doped-ZnS ceramic powder. Solid State Sci 14:299–304
36. Chang S-Q, Kang B, Dai Y-D, Zhang H-X, Chen D (2011) One-step fabrication of biocompatible chitosan coated ZnS and ZnS: Mn^{2+} quantum dots via gamma-radiation route. Nanoscale Res Lett 6:591
37. Wageh S, Ling ZS, Xu-Rong X (2003) Growth and optical properties of colloidal ZnS nanoparticles. J Cryst Growth 255:332–337
38. Tarasov K, Houssein D, Destarac M, Marcotte N, Gérardin C, Tichit D (2013) Stable aqueous colloids of ZnS quantum dots prepared using double hydrophilic block copolymers. New J Chem 37: 508–514
39. Zheng Y, Gao S, Ying JY (2007) Synthesis and cell imaging applications of glutathione-capped CdTe quantum dots. Adv Mater 19: 376–380
40. Barman B, Sarma KC (2011) Luminescence properties of ZnS quantum dots embedded in polymer matrix. Chalcogenide Lett 8: 171–176
41. Xue Z, Shengjiang W, Weijia Z, Jichuan Q, Yongzhong W, Hongzhi L, Chengwei X, Xiaopeng H (2014) Highly biocompatible POSS-coated CdTe quantum dots for cell labeling. RSC Adv 4:598
42. Rozenberg BA, Tenne R (2008) Polymer-assisted fabrication of nanoparticles and nanocomposites. Prog Polym Sci 33:40–112